Problems with Hu-Duan Boundary Effect Model and Its Comparison to Size-Shape Effect Law for Quasi-Brittle Fracture

Qiang Yu[1]; Jia-Liang Le[2]; Christian G. Hoover[3]; and Zdeněk P. Bažant[4]

Abstract: Recent disagreements on the mathematical modeling of fracture and size effect in concrete and other quasi-brittle materials are obstacles to improvements in design practice, and especially in design codes for concrete structures. In an attempt to overcome this impediment to progress, this paper compares the Hu-Duan boundary effect model (BEM) expounded since 2000 to the size-shape effect law (SEL) proposed at Northwestern University in 1984 and extended to the geometry (or shape) effects in 1990. It is found that within a rather limited part of the range of sizes and shapes, the fracture energy values identified by BEM and SEL from the test data on maximum loads are nearly the same. But in other parts of the range the BEM is either inferior or inapplicable. The material tensile strength values identified by BEM have a much larger error than those obtained from the SEL after calibration by the cohesive crack model. From the theoretical viewpoint, several hypotheses of BEM are shown to be unrealistic.

DOI: 10.1061/(ASCE)EM.1943-7889.89

CE Database subject headings: Cracking; Concrete; Structural failures; Data analysis; Size effect.

Author keywords: Fracture scaling; Fracture energy; Concrete; Asymptotics of fracture; Cohesive cracks; Failure of structures; Evaluation of experimental data.

Introduction

The nominal strength of a structure is a load parameter defined as $\sigma_N = P/bD$ or P/D^2 for two- or three-dimensional similarity; P = maximum load (or its parameter), D = structure size, and b = thickness of a two-dimensionally similar structure. If the material failure criterion is defined solely in terms of material strength or critical strain, and if the material strength randomness is neglected, then geometrically similar structures of different sizes D have the same σ_N. Thus any dependence of σ_N on D came to be known as the size effect.

After Weibull (1939,1951) formulated his mathematical theory of the statistical size effect, every experimentally observed size effect was perceived as statistical. However, the emergence of an energetic theory of size effect in quasi-brittle structures (Bažant 1984,2004,2005) has gradually changed this perception. Recently, though, another nonstatistical theory has been championed by Hu and Duan (2008,2010). The goal of the present study is to compare these two theories.

By the late 1990s, the majority of members of the committees preparing concrete design codes became persuaded that the size effect should, in principle, be somehow taken into account. But this important goal has so far been frustrated by disagreements on the theory. Hopefully the present analysis would help to resolve this impasse and move toward better codes.

Summary of Energetic Size-Shape Effect Law

Size Effect in Structures with Large Cracks or Notches (Type 2)

A deterministic size effect in quasi-brittle structures is caused by energy release due to stress redistribution by growing fracture. This size effect is of two basic types. The SEL of Type 2, researched first (Bažant 1984,1997,2004), applies to structures that have a deep notch or contain at peak load a large traction-free (i.e., fatigued) crack. It reads

$$\sigma_N = \hat{B} f_t' \left(1 + \frac{D}{D_0}\right)^{-1/2} \quad \text{(Type 2 SEL)} \tag{1}$$

where

$$D_0 = c_f g'(\alpha_0)/g(\alpha_0), \quad \hat{B} f_t' = \sqrt{EG_f/g'(\alpha_0)c_f} \tag{2}$$

where f_t' = material tensile strength; E = Young's elastic modulus; $\alpha_0 = a_0/D$, a_0 = initial crack or notch length; D_0 = transitional size; $\alpha = a/D$; $a = a_0 + c_f$; $g(\alpha) = K_I^2 D(b/P)^2$ = dimensionless energy release function of linear elastic fracture mechanics (LEFM); K_I = mode I stress intensity factor; G_f = initial fracture energy (i.e. area under the initial tangent of the softening curve $\sigma(w)$ of co-

[1]Postdoctoral Research Associate, Northwestern Univ., Evanston, IL 60208.

[2]Graduate Research Assistant, Doctoral Candidate, Northwestern Univ., Evanston, IL 60208.

[3]Graduate Research Assistant, Doctoral Candidate, Northwestern Univ., Evanston, IL 60208.

[4]McCormick Institute Professor, W.P. Murphy Professor of Civil Engineering and Materials Science, Northwestern Univ., 2145 Sheridan Rd., CEE/A135, Evanston, IL 60208 (corresponding author). E-mail: z-bazant@northwestern.edu

Note. This manuscript was submitted on August 10, 2009; approved on September 8, 2009; published online on December 15, 2009. Discussion period open until June 1, 2010; separate discussions must be submitted for individual papers. This paper is part of the ***Journal of Engineering Mechanics***, Vol. 136, No. 1, January 1, 2010. ©ASCE, ISSN 0733-9399/2010/1-40–50/$25.00.

hesive stress σ versus crack opening w; Bažant et al. 2002; Bažant 2005); and c_f=material length constant representing the distance from crack tip to the resultant of tensile stresses in the fracture process zone (FPZ), and is proportional to the Irwin's material characteristic length $l_{ch}=EG_f/f_t'^2$ (Irwin 1958), pioneered for concrete by Hillerborg et al. (1976). Eq. (1) applies only if the structure has a positive geometry, i.e. is such that $g'(\alpha_0)>0$. In coordinates $X=D\ g(\alpha_0)/g'(\alpha_0)$ and $Y=1/\sigma_N^2 g'(\alpha_0)$, SEL Eq. (1) gives a linear regression plot $Y=AX+C$, from which A and C can be identified as the slope and intercept. Then $G_f=1/AE$ and $c_f=C/A$ (Bažant and Kazemi 1990a; Bažant 2005). $G_f\approx 0.2$ to 0.5 of the total fracture energy G_{fT}, which represents the total area under the $\sigma(w)$ curve; G_{fT} (elsewhere normally denoted as G_F) is commonly measured by the work-of-fracture method, proposed by Nakayama (1965) and Tattersall and Tappin (1966), later pioneered for concrete by Hillerborg (1985) (RILEM 1985). The coefficient of variation of G_{fT} is about twice as large as that of G_f (Bažant and Becq-Giraudon 2002).

Eq. (2), proposed in 1990 (Bažant and Kazemi 1990a,b), introduces into the SEL through $g(\alpha)$ the structure geometry effect. Accordingly, the name "size-shape effect law" (SEL) is more appropriate and has occasionally been used, although the shorter original term "size effect law" seems to have stuck. The SEL has been shown to fit the test data on many quasi-brittle materials quite well [see the reviews in Bažant (2005), and Bažant and Planas (1998)], and has been supported by numerical simulations, especially those with the cohesive crack model.

Size Effect for Crack Initiation (Type 1)

The Type 1 SEL applies to quasi-brittle structures of positive geometry failing at crack initiation from a smooth surface. Because of material heterogeneity, a finite cracking zone representing the FPZ must develop before the cracking can coalesce into an initial macrocrack of finite depth attached to the surface. The formation of the initial FPZ causes stress redistribution and energy release necessary to drive the macrocrack. The Type 1 SEL reads (Bažant and Li 1996; Bažant 2005):

$$\sigma_N=\sigma_\infty\left(1+\frac{rD_b}{D}\right)^{1/r} \tag{3}$$

where $D_b=\langle -g''(0)c_f/4g'(0)\rangle$ and $\sigma_\infty=[EG_f/c_f g'(0)]^{1/2}$ where $\langle x\rangle=\max(x,0)$, r=empirical parameter $(0.5<r<2)$, σ_∞=constant, and $D_b\approx$ double the thickness of the boundary layer of cracking in beam flexure. The curve of Type I SEL terminates for large sizes with a horizontal asymptote because, for large D, the FPZ size $\ll D$. Due to the randomness of material strength, a macrocrack can, of course, initiate at many different points in the structure, which causes that, for $D\gg l_{ch}$, the Weibull power-law statistical size effect becomes dominant and leads to a final asymptote of downward inclination in the logarithmic plot. A generalized Type 1 SEL, amalgamating both the deterministic (energetic) and statistical size effects, has been derived from the nonlocal Weibull theory (Bažant and Xi 1991); it reads (Bažant and Novák 2000a,b): $\sigma_N=\sigma_\infty[(l_s/D)^{rn/m}+rD_b/D]^{1/r}$ where m=Weibull modulus and $n=1$, 2, or 3 for uni, two-, or three-dimensional similarity of fracture. For small sizes, this equation converges to Eq. (3), and for large sizes it converges to Weibull's size effect, i.e., $\sigma_N\propto D^{-n/m}$ [for probabilistic analysis of Type 1 SEL, see Bažant and Pang (2006,2007) and Bažant et al. (2009)].

Summary of Hu-Duan Boundary Effect Model

The boundary effect model (BEM), whose latest description is found in Hu and Duan (2008,2010), attributes the size effect on structural strength to the interaction between the fracture process zone (FPZ) and the structural boundary. The effect of crack length on the specimen strength is approximated as a smooth transition between two asymptotic cases: (1) when the crack length $a\to 0$, the nominal strength, representing the maximum stress in the specimen at peak load, is considered to approach the material tensile strength f_t'; (2) when a and $(D-a)$ are sufficiently large, the specimen strength follows the LEFM. For the transition, it is postulated that (Hu and Duan 2007,2008,2010; Hu and Wittmann 2000)

$$\sigma_N=\frac{f_t'}{\sqrt{1+a/a_\infty^*}} \tag{4}$$

where $a_\infty^*=l_{ch}/1.12^2\pi$; $l_{ch}=(K_{IC}/f_t')^2$=Irwin's characteristic length (Irwin 1958); K_{IC}=critical K_I (fracture toughness); and a=crack length without the FPZ length (identical to a_0 in the SEL). To extend Eq. (4) to small ligaments for which the crack front approaches the opposite boundary (Duan and Hu 2004; Duan et al. 2006; Hu and Duan 2007,2008,2010), the nominal strength is redefined as $\sigma_n=\sigma_N/A(\alpha)$ where $\alpha=a/D$ and D=width of cross section with the crack, denoted as W by Hu and Duan, and $A(\alpha)$=dimensionless factor such that σ_n represent the stress for peak load at the crack tip under the hypothesis of a linear stress distribution across the ligament, the crack tip stress singularity being ignored (Duan and Hu 2004; Duan et al. 2006). For example, for three-point bend (3PB) specimen, $\sigma_N=3PS/2bD^2$ and $A(\alpha)=(1-\alpha)^2$ (where S is the span of beam); for single-edged notched specimen, $\sigma_N=P/bD$, and $A(\alpha)=(1-\alpha)^2/(1+2\alpha)$.

Two asymptotic limits are imposed on the σ_n: (1) material strength criterion: $\sigma_n=f_t'$ for $\alpha=0$ or $\alpha=1$; and (2) LEFM criticality criterion: $\sigma_n=K_{IC}/[A(\alpha)Y(\alpha)\sqrt{\pi a}]=f_t'/\sqrt{a_e/a_\infty^*}$ for $D/l_{ch}\to\infty$, $a/l_{ch}\to\infty$, and $(D-a)/l_{ch}\gg 1$ where $a_e=B(\alpha)a$; $B(\alpha)=[A(\alpha)Y(\alpha)/1.12]^2$; $Y(\alpha)=k(\alpha)/\sqrt{\pi\alpha}$; and $B(\alpha)$, $Y(\alpha)$=geometry dependent dimensionless parameters (these asymptotic conditions are actually not explicitly stated by Hu and Duan, but they are implied).

To obtain a continuous transition between the aforementioned asymptotic limits of σ_n, a formula analogous to the Type 2 SEL is again postulated

$$\sigma_n=\frac{f_t'}{\sqrt{1+a_e/a_\infty^*}}\quad\text{or}\quad\sigma_N=\frac{A(\alpha)f_t'}{\sqrt{1+a_e/a_\infty^*}} \tag{5}$$

Furthermore, Hu (2002) and Duan et al. (2006) considered the fracture toughness and fracture energy to be variable parameters and, based on Eq. (5), they assumed a size dependent fracture toughness in the form $K_C=\sigma_N Y(\alpha)\sqrt{\pi a}$. Then, using Eq. (5), they proposed the formula

$$\frac{K_C}{K_{IC}}=\sqrt{\frac{a_e/a_\infty^*}{1+a_e/a_\infty^*}} \tag{6}$$

For geometrically similar specimens, this expression led to the following size effects on fracture toughness and fracture energy (Hu and Wittmann 2000; Hu 2002)

$$K_C = \sqrt{\frac{A_1 D}{1 + B_1 D}}, \quad G_f = G_F \frac{B_1 D}{1 + B_1 D} \tag{7}$$

where $G_f = K_C^2/E$ (Irwin's relation); $A_1 = \alpha B(\alpha) K_{IC}^2 / a_\infty^*$; and $B_1 = \alpha B(\alpha)/a_\infty^*$.

Problematic Physical and Mathematical Aspects of the Boundary Effect Model

1. *Incorrect hypothesis about the FPZ-boundary interactions and size effect mechanism.* Hu and Duan (2008) assert that (1) "the size-dependent quasi-brittle fracture transition is actually due to the interaction of FPZ with the nearest structure boundary rather than the size variation," and that (2) "the widely accepted SEL for geometrically similar specimens of different sizes is only a special case of quasi-brittle fracture controlled by the FPZ/boundary interaction." Both assertions are untrue. When the ligament length $(D-a)$ and the crack length a are both much larger than the FPZ length, one has $D \gg c_f$ (or $D/D_0 \gg 1$) which gives the strongest size effect possible—the size effect of the LEFM (i.e. $\sigma_N \propto D^{-1/2}$). Yet in that case there is no interaction with the boundary because the FPZ is surrounded by the LEFM near-tip stress field, which is independent of the boundary geometry. When the ratio of FPZ length to $(D-a)$ increases while $(D-a)/D$ is nonvanishing, the size effect weakens (or D/D_0 is not $\gg 1$). In that case, the increasing proximity of the boundary mitigates the size effect. On the other hand, when the ligament $(D-a)$ is negligible compared to D while D is changed at constant ratio $(D-a)/D$, the size effect is getting stronger, approaching again the LEFM size effect. Hence, the FPZ-boundary interaction can either mitigate or enhance the size effect, and thus cannot be the cause of size effect (see also the cohesive stress analysis that follows; Cedolin and Cusatis 2008; Cusatis and Schauffert 2009).
2. *Disregard of energy balance condition.* If σ_N and the structure geometry are kept constant, the calculated rate of energy release from the structure increases with structure size D. To ensure that it remain equal to the rate of energy dissipation in the FPZ of a crack, σ_N must decrease with increasing D (Bažant 1984,2004,2005). The derivation of BEM ignores this undeniable source of size effect.
3. *Ambiguity of stress profile definition and of* σ_n. When only the typical Mode I fracture specimens are considered and the specimen geometry, including the ratio a/D, does not change, the values of σ_n and σ_N are proportional and thus equivalent, and the size effects the same. However, the definition of σ_n and of the stress profile across the ligament becomes ambiguous when extended beyond a few basic types of Mode I fracture specimens; see all the nonunique and dubious linear stress profiles across the ligaments sketched in Fig. 1. For all these examples, $A(\alpha)$ cannot be objectively calculated. E.g., mixed mode fracture may occur, or the direction angle ϕ in which the ligament will crack is a priori unclear [Figs. 1(a–c)], or the ratio of bending moment M to normal force N in the ligament is statically indeterminate [Figs. 1(d and f)], or the stress profile cannot even be defined [Figs. 1(e, g, and h)]. On the other hand, function $g(\alpha)$ on which the SEL is based can be unambiguously calculated for all these cases.
4. *Incorrectness of linear stress profile at varying a and in asymptotic cases.* The linear stress profile [Fig. 2(a)] is usable only if it gives a constant ratio σ_n/σ_N. This can happen only when the real stress profiles [Fig. 2(a)] remain similar, which is not the case when a is varied, and especially not when D is small. Eq. (5) incorrectly predicts $\sigma_n = f_t'$ when $D/l_{ch} \to 0$ and $a_e \to 0$ (i.e., $a/D \to 0$ or $a/D \to 1$). But for these cases the actual f_t' is very different from σ_n [based on Eq. (5)] because a rectangular stress profile must be approached. The reason is that for $D \to 0$ the crack openings at peak load are infinitely small, making the cohesive stresses nearly equal to f_t' at all points, so that the cohesive crack model becomes asymptotically equivalent to a crack filled by a glue perfectly plastic in tension [Fig. 2(c)]. Equally problematic is the BEM assumption of a linear stress profile across a vanishing ligament $a-D$, for all D. Here the peak load is reached while the opening displacements are small everywhere, causing the cohesive stress profile to be almost rectangular.
5. *Problematic definition of* a_e. In BEM, the asymptotic cases of crack initiation from the surface and of vanishing ligament are amalgamated by the hypothesis of an equivalent crack length a_e [Fig. 2(b) in Duan et al. 2006]. However, this hypothesis is predicated on the assumption of a linear stress profile, already discussed.
6. *No mathematical basis for asymptotic matching.* Although, in setting up the BEM, the two asymptotes were matched, the

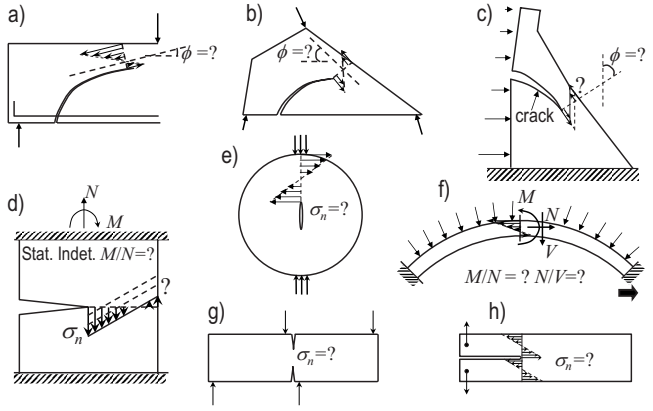

Fig. 1. Examples of specimens and structures for which SEL can be used but BEM cannot

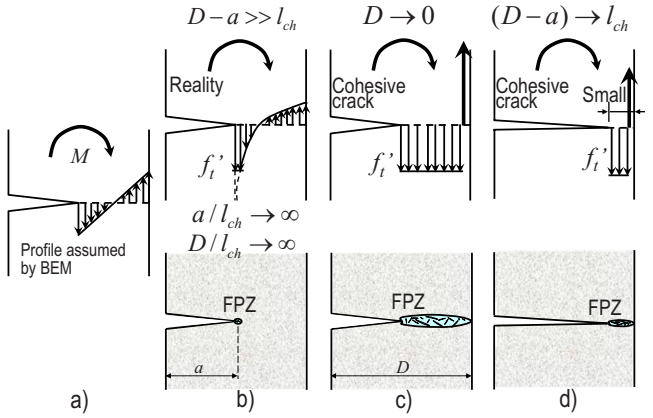

Fig. 2. [(a) and (b)] Stress distributions along the ligament contrasting BEM versus reality; (c) distributions for vanishing size; and (d) for vanishing ligament, with corresponding fracture process zones

procedure was intuitive and no use was made of any systematic procedure to match the two-sided second-order asymptotic properties characterizing the way the asymptotes are approached. For example, instead of Eq. (4), the intuitive procedure used in BEM would also allow using, e.g., $\sigma_n = f'_t/(1+\sqrt{a/a^*_\infty})$, or $f'_t[1+(a/a^*_\infty)^{1/2r}]^{-r}$ (with any positive r), or various smooth exponential transitions, which all have the same asymptotes. It seems that the tacit reason for picking the expressions in Eqs. (4) and (5) was a need to agree in the usual testing range with Eq. (1) of the Type 2 SEL. This equation was derived by matching the second-order asymptotic properties required by cohesive crack model (Bažant 2001,2004,2005), or by equivalent LEFM (Bažant 1997), or by energy release analysis of special cases (Bažant 1984).

7. *Ranges of agreement and disagreement between BEM and SEL.* It was claimed that the SEL was a special case of BEM (Hu and Duan 2008,2010). This claim is baseless. For normal depth notches and large enough sizes (such that $a \gg l_{ch}$ and $(D-a) \gg l_{ch}$), the size effects of BEM and SEL are, of course, the same. But this happens only because the transition between the asymptotic cases is characterized by formulas (4) and (5) that have the same form as the SEL. However, unlike SEL, BEM is unusable for general structures (Fig. 1). Because of incorrect asymptotics and the linear stress profile already discussed, the BEM differs from SEL in a major way and gives incorrect results for very small sizes, vanishing ligaments, shallow notches, and notchless specimens. Comparisons with experiments and cohesive crack calculations bear it out.
8. *Unrealistic hypothesis of proportionality of flaw size to structure size.* In absence of any preexisting crack, the BEM, like LEFM, would predict, according to Eq. (5) no size effect for failures at crack initiation (Type 1). Since the BEM does not consider the development of a finite FPZ at the surface, the problem is circumvented by postulating that some finite initial crack always exists, even if the surface is smooth. This initial crack is considered to be the largest among the randomly distributed preexisting flaws (Hu and Duan 2008). The same idea was proposed by Freudenthal (1968), but for a different purpose, namely to provide a microstructural basis for Weibull's statistical size effect theory.

   The BEM borrows that theory but without statistics. To explain why larger unnotched structures failing at crack initiation exhibit a smaller σ_N, the BEM assumes the size of the largest flaw to be proportional to the structure size D (Hu and Duan 2008,2010). But this hypothesis is flawed. If, for instance, the size of the largest flaw in a 15-cm-deep test beam is 1 cm, one would have to assume that the size of inevitable flaws in the 6-m-deep unreinforced plinth of the failed Schoharie Creek Bridge reached 0.4 m. That agrees neither with observations, nor with statistics. The flaw size distribution is strictly a material property and thus cannot be a function of the structure size. Although, according to the flaw size distribution, the size of the largest statistically expected flaw increases with structure size, it increases much slower than proportionally. So, if Hu and Duan were right, the Freudenthal (1968) analysis relating the flaw size distribution to the statistical size effect in structures would yield a Weibull statistical distribution in which the shape and scale parameters would be size dependent. Yet they are not.

   The real reason for the deterministic and statistical parts of Type 1 size effect is that, because of heterogeneity, a FPZ (or a cracking zone) of a certain finite size must form before a macrocrack can grow, and that this finite FPZ, having random strength, can form randomly at different locations (Bažant and Pang 2006,2007; Bažant et al. 2009).
9. *Incorrect large-size asymptote for failures at crack initiation.* In the BEM, the size effect on nominal strength at $a=0$ is expressed by Eq. (5), which is very different from the deterministic Type 1 SEL [Eq. (3)], especially for the large size asymptote. For $D \to \infty$, the deterministic Type 1 size effect law terminates with a horizontal asymptote (this has been mathematically proven either by expanding the energy release rate function or by calculating the stress redistribution caused by a boundary zone of cracking). By contrast, the BEM predicts the size effect at crack initiation in geometrically similar structures to be $\sigma_N \propto D^{-1/2}$. But this is the same as the LEFM size effect for large similar cracks, which cannot apply to cracks smaller than the finite cracking zone (FPZ).

   In some recent papers (Hu and Duan 2008,2010), it has been argued that Eq. (5) of BEM can fit the experimentally observed Type 1 data. However, the size range of the test data fitted (Hu and Duan 2008,2010) was rather limited compared to the scatter band width. For a broader range, better fits would be obtained with the Type 1 SEL.
10. *Absence of statistical part of size effect at crack initiation.* For very large sizes, i.e. $D/l_{ch} \gg 1$, concrete structures such as arch dams must exhibit the Weibull power-law statistical size effect, $\sigma_N \propto D^{-n/m}$, where m=Weibull modulus and n =number of dimensions of fracture scaling (1, 2, or 3). The Weibull size effect is included in the complete SEL formulation (Bažant and Yu 2009; Bažant and Novák 2000b; Bažant et al. 2007; RILEM TC QFS 2004) but is missing from the BEM. As for smaller sizes, the Weibull power-law does not apply, but it would be a mistake to think that the statistical part of size effect is absent. Combined though it is with the deterministic size effect, it is in fact represented by the weakest-link model with a finite number of links (Bažant et al. 2009; Bažant and Pang 2007).
11. *Identification of material strength and its error in BEM.* Is identification of f'_t an advantage of BEM? Not really. It will be shown that, contrary to the claims by Hu and Duan (2008,2010), the value of f'_t can be identified from the SEL parameters c_f, G_f, and E, and that the f'_t value identified from the BEM is incorrect (having errors $\sim$70%).
12. *Size effect on apparent fracture toughness or fracture energy, and R-curve.* It has been claimed (Hu and Wittmann 2000; Hu 2002; Duan et al. 2006) that the BEM has the advantage of being able to capture the variability of fracture energy for small a/l_{ch} and small $(D-a)/l_{ch}$. This claim, however, is misleading for two reasons:
    a. What is variable is not fracture energy G_F but the *apparent* fracture energy $\tilde{G}_f$ evaluated by classical methods that do not take into account the finiteness of the FPZ caused by material heterogeneity (Bažant 1996; Bažant and Yu 2004).
    b. As shown by Rice in 1968 (Rice 1968), the work integral $G_F = \int_{w=0}^{\infty} \sigma(w) dw$ defining the fracture energy of a cohesive crack is equal to the flux of energy into the FPZ of a propagating crack, given by Rice's J-integral. However, this is true only for quasi-steady crack propagation, during which the stress and strain fields immediately surrounding the FPZ do not change. Near the tip

of notch or initial stress-free (fatigued) crack and near the opposite boundary, the propagation is not steady, and the energy flux J required to propagate the crack is smaller than G_F; in detail see Bažant and Yu (2004). When the testing method gives J, or the average J over the ligament (Nakayama 1965; Hillerborg 1985; RILEM 1985), it is not surprising that the fracture energy appears to be variable.

The variation of apparent fracture energy near the notch tip, generally called the R-curve (or resistance curve), can approximately be determined from the SEL, using a constant fracture energy G_f

$$\tilde{G}_f = G_0 \frac{D}{D+D_0}, \quad \tilde{K}_C = K_C \sqrt{\frac{D}{D+D_0}} \tag{8}$$

where $G_0 = G_f g(\alpha)/g(\alpha_0)$ and $\tilde{K}_C = \sqrt{E\tilde{G}_f}$ [see Eq. (14) derived in Bažant and Kazemi (1990a)]. This is equivalent to Eq. (7) of the BEM, although in the sense of the apparent, rather than the real, fracture energy. So, the idea of a size-dependent fracture energy is an artificial and unnecessary complication.

The apparent fracture energy also varies with crack extension from the notch. This variation is called the R-curve (resistance curve). Is BEM needed to describe it (Hu and Wittmann 2000)?—not quite. The R-curve can be derived from the SEL [see Eqs. (27)–(28) in Bažant and Kazemi (1990b)]. Moreover the SEL also yields the dependence of the R-curve on the specimen geometry (or shape).

Comparisons with Experimental Evidence

The column diagrams in Fig. 3 compare the material fracture parameters obtained by fitting the Tang et al. (1996) tests of notched 3PB beams and single edge-notched eccentrically compressed (EC) prisms, cast from two concrete batches, I and II. For beams, both the size and the notch-depth ratio were varied, while for prisms only the notch-depth ratio was varied. Utilizing the SEL, one can estimate K_{IC}, G_f, and c_f by linear regression of $1/\sigma_N^2$ versus D. For the BEM, one can get f_t' and K_{IC} by similar linear regression. For both SEL and BEM, one set of parameters is obtained by fitting the 3PB tests and another set by fitting the EC tests. For comparisons, the parameter sets for 3PB are considered as the basis and their values are written on the columns. The ratios of the parameters for the EC tests to the 3PB parameters are shown by the columns in Fig. 3.

If SEL and BEM were perfect, the heights of the columns corresponding to these models would all be 1. So the deviations from 1 represent errors caused by changing the test geometry from 3PB to EC. The column diagrams show that, for Batch I, the errors for SEL are very small. The error of f_t' for BEM is huge (73%) and K_{IC} cannot even be calculated because the linear regression slope is negative. For Batch II, the performance of BEM for f_t' is equally poor and K_{IC} again does not exist. The performance of SEL for batch II becomes mixed; for K_{IC} and G_f the errors are still small, but for c_f the error becomes big. Overall, the SEL clearly scores better.

Fig. 4 shows all the σ_N values measured by Tang et al. in dimensionless size effect plots of nominal strength versus size [for BEM, $W^* = a_\infty^*/\alpha B(\alpha)$]. If both methods were perfect and the random scatter were nil, all the experimental points would lie on the curve. Evidently, the plot for SEL is more consistent than it is for BEM.

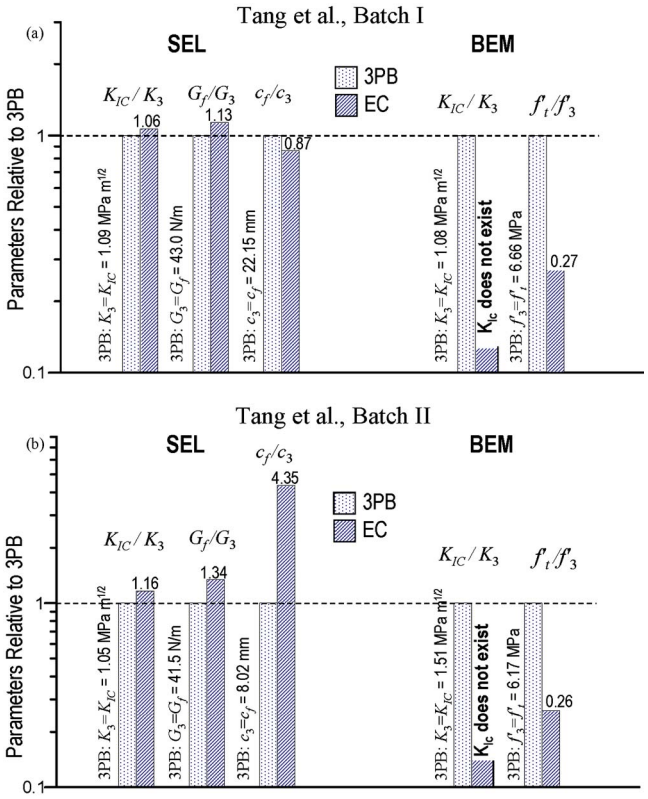

Fig. 3. Analysis of the Tang et al. (1996) tests: (a) Batch I; (b) Batch II

Fig. 5 shows similar comparisons for Karihaloo et al. (2003) 3PB tests. These tests, used repeatedly in several Hu and Duan's papers, were made for hardened cement paste (HCP) (which is perfectly brittle) and for high strength concrete (HSC) (which is rather brittle). Since the brittle behavior can be perfectly predicted from LEFM, the high brittleness diminishes the relevance of these tests to quasi-brittle materials, which are here the main objective. Anyway, the material parameters of both SEL and BEM are calibrated from the measured maximum loads for various beam sizes (whose ratios were 1:2:4) and for the same relative notch depth of $\alpha_0 = 0.3$.

Fig. 5(a) shows the comparison of HCP beams with relative notch depths $\alpha_0 = 0.05$, 0.1, 0.3, and 0.5. For SEL, the results for shallow notches $\alpha_0 = 0.05$ and 0.1 are worse than those for $\alpha_0 = 0.3$ and 0.5, but this is not at all surprising because the SEL was

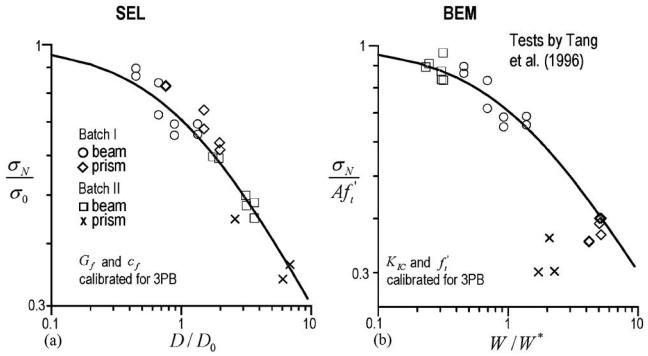

Fig. 4. Dimensionless size effect plots of the Tang et al. (1996) tests: (a) SEL; (b) BEM

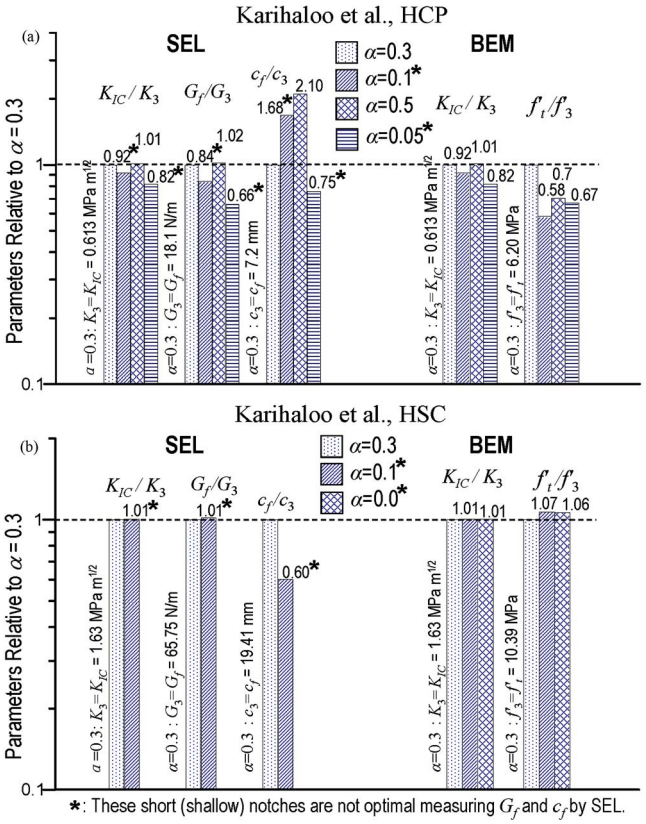

Fig. 5. Analysis of the Karihaloo et al. (2003) tests: (a) HCP; (b) HSC

not recommended for such shallow notches as they belong to the transition of Type 1 to Type 2. As seen in Fig. 5, c_f is the more inconsistent parameter of the SEL. For BEM, the tensile strength f_t' is equally inconsistent. For example, the BEM tensile strength f_t' for $\alpha_0=0.1$ is only 58% of what BEM gives for $\alpha_0=0.3$.

Note, though, that the results for such shallow notches should be properly be fitted by the universal SEL which can describe this transition (Bažant and Yu 2009), but with more complicated formulas. This transitional range is actually unsuitable for testing G_f since the σ_N values depend mainly on f_t' and are only weakly sensitive to G_f. Thus, even though the results for SEL for these shallow notches are included in Fig. 5, they cannot be regarded as a fair comparison of SEL to BEM.

Fig. 5(b) shows beams made of HSC. Three size effect test series, with $\alpha_0=0$, 0.1 and 0.3, were carried out. The notchless beams ($\alpha_0=0$) require the Type 1 SEL described by Eq. (3), but this equation is unsuitable for extracting G_f. Therefore, only the beams with deeper notches, $\alpha_0=0.1$ and 0.3, with the Type 2 SEL [Eq. (1)], can be used to identify K_C, G_f, and c_f. Therefore, in Fig. 5, one can obtain K_{IC}, G_f, and c_f from the SEL only for $\alpha_0=0.1$ and 0.3. The deeper notch $\alpha_0=0.3$ is more effective since it lies farther from the range of transition between Types 1 and 2.

Fig. 6 is analogous to Fig. 4 except that the data are those measured by Karihaloo et al. (2003). Here the plot of BEM is slightly more consistent.

Fig. 7 shows similar column diagrams for the size effect tests of Bažant and Pfeiffer (1987). Fig. 7(a) corresponds to a concrete with aggregate size ≤12.7 mm. The tests were made for 3PB, double notched tension (DNT), and double notched eccentric compression (DNC). Since function $g(\alpha)$ for DNC is not found in handbooks, elastic finite-element analysis has been undertaken to

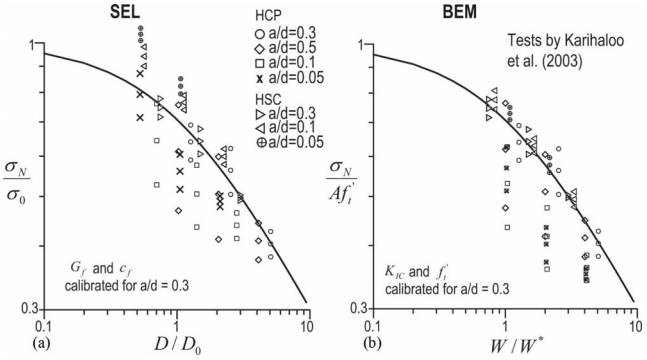

Fig. 6. Dimensionless size effect plots of the Karihaloo et al. (2003) tests: (a) SEL; (b) BEM

calculate the $g(\alpha)$; the result is $g(\alpha_0)=1.54$ and $g'(\alpha_0)=6.86$. For SEL, the parameters except c_f are seen to be quite consistent. For BEM, both K_{IC} and f_t' deviate considerably.

Fig. 7(b) shows Bažant and Pfeiffer's size effect tests of 3PB, DNT, and DNC on mortar. Note that, for the SEL, the K_{IC} and G_f values are very consistent while c_f for DNT deviates very much. The likely reason is the relatively greater randomness of the tests with mortar, causing high scatter in the regression line intercept. For the BEM, both K_{IC} and f_t' deviate considerably. Overall, the SEL scores in these tests again better.

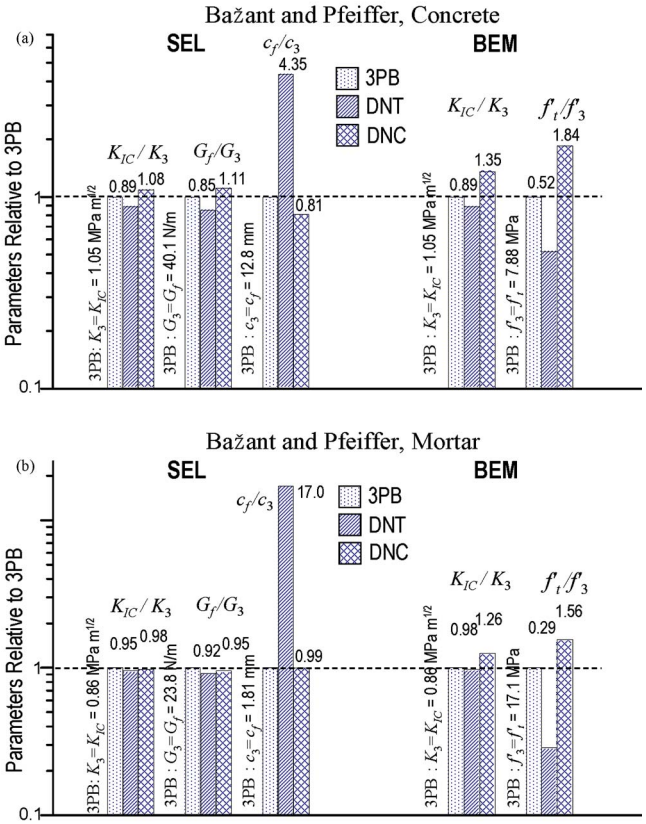

Fig. 7. Analysis of the Bažant and Pfeiffer (1987) tests: (a) concrete specimens with aggregate size ≤12.7 mm; (b) mortar specimens

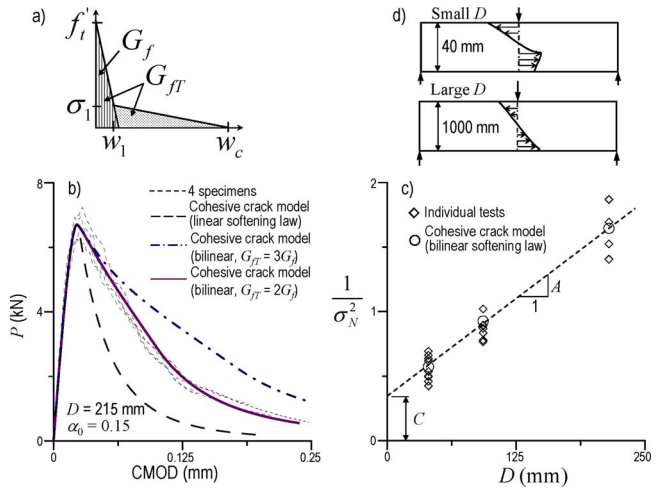

Fig. 8. (a) Cohesive crack model with a bilinear softening stress-separation law; (b)simulation compared with the recorded load-CMOD curves; (c) comparison of peak loads between simulations and tests; and (d) normal stress profiles in small and large notchless beams

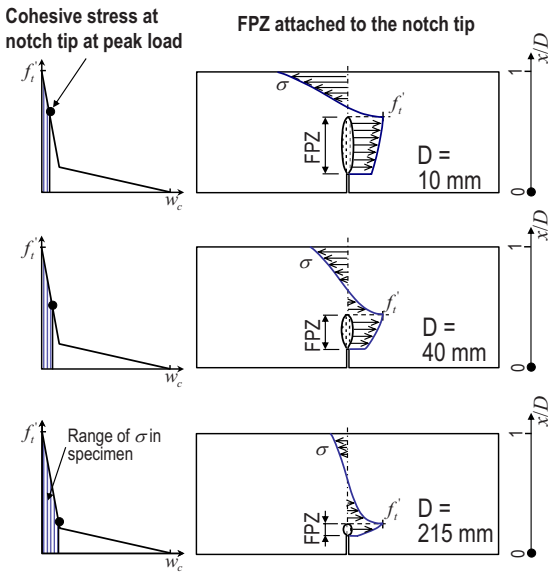

Fig. 9. FPZ and cohesive stress at notch tip at peak load for beams of different sizes

New Size Effect Tests Enhanced by Load-CMOD Curves and Cohesive Crack Simulations

The scope and range of the existing test data is, unfortunately, quite limited but can be extended by applying the cohesive crack model, a model that has been proven to be highly realistic for quasi-brittle fracture. This model was proposed by Barenblatt (1959), finalized by Rice (1968) who proved the equality of work of fracture to energy flux, and pioneered for concrete by Hillerborg et al. (1976), Petersson (1981), and Hillerborg (1985) under the alternative name "fictitious crack model."

As is well known, the postpeak load-deflection response can be represented realistically if a bilinear stress-displacement curve $\sigma(w)$ [Fig. 8(a)] is used. Within the normal range of sizes and crack lengths, the cohesive stresses in the FPZ at maximum load remain entirely within the initial linear portion, and so the tail of the softening $\sigma(w)$ curve cannot be obtained by testing the maximum loads only. This limitation applies not only to the SEL based testing but also to the BEM based testing because it means that the BEM predictions are independent of the form of the tail of $\sigma(w)$. Consequently, the tests of SEL as well as BEM must be supplemented by knowledge of the complete load-deflection curve. Unfortunately, none of the test data used here include the postpeak deflections.

Therefore, new concrete fracture tests on 3PB beams have been carried out at Northwestern University. *Test details:* ready-mixed concrete procured from Ozinga, Inc., Chicago. Contents per cubic yard concrete: 470 lb of Type I cement, 1.20-lb fly ash, 1,680-lb coarse aggregate of maximum size 9.5 mm, 1,540-lb fine aggregate, and 207-lb water. The specimens were demolded 1 day after casting and then stored in standard curing room for 68 days until the time of test. The notches were cut by a diamond saw 1 month after the casting. Compression tests on standard cylinders cast from the same concrete showed at the time of tests mean $E \approx 30$ GPa and compression strength $f_c'=41$ MPa. Tested within 4 days were ten specimens of $D=40$ mm, giving the peak loads of 1,967, 2,007, 2,261, 2,037, 2,008, 2,273, 2,456, 1,922, 2,361, and 2,185 N; seven specimens of $D=93$ mm, giving the peak loads of 3,988, 3,942, 3,683, 3,932, 4,069, 4,249, and 4,214 N; and four specimens of $D=215$, giving the peak loads of 6,290, 7,253, 6,965, and 6,609 N.

To obtain wider ligaments, which minimize interaction with the opposite boundary (invoked by Hu and Duan), a relatively low notch-depth ratio $\alpha_0=0.15$ was selected. The beams were geometrically similar, of depths $D=40$, 93, and 215 mm. They were tested under crack-mouth opening displacement (CMOD) control and were simulated using the cohesive crack model with a bilinear $\sigma(w)$. By using a finite-element fracture code to fit both the measured maximum loads for all D and the measured complete load-CMOD curve, the following $\sigma(w)$ parameters defined in Fig. 8(a) were identified: $f_t'=4.80$ MPa, $w_c=8.0\times10^{-5}$ m, $\sigma_1=0.2\ f_t'=0.96$ MPa, and $w_1=1.07\times10^{-5}$ m.

Figs. 8(b and c) documents an excellent fit of both the experimental load-CMOD curves for $D=215$ mm and the nominal strengths σ_N for all the three sizes. The cohesive crack model in Fig. 8(a) is thus validated. Note that the bilinear $\sigma(w)$ is fixed by the position of the knee point (w_1,σ_1) and the ratio G_{fT}/G_f. If the tail of $\sigma(w)$ is dropped (i.e. $G_{fT}/G_f=1$) and the cohesive law is assumed to be linear, the σ_N values for the three sizes are still matched, but the load-CMOD curve descends far too steeply, as shown by the dashed curve in Fig. 8(b). Contrarily, if the slope of the tail is reduced to get $G_{fT}/G_f=3$, then the load-CMOD curve will descend far too slowly; see the dash-dotted line in Fig. 8(b). The explanation is that the cohesive stresses in the FPZ do not enter the tail within the size range considered; see Fig. 9. If the stress profile along the ligament at peak load is plotted, it can be seen in Fig. 9 that the FPZ is located far away from the boundaries. This further invalidates the BEM hypothesis about the FPZ-boundary interaction.

The nominal strength values for beams with no notch but otherwise the same shape are then numerically simulated using the same cohesive crack model. If these simulations are extended up to the depth of $D=1$ m (Fig. 10(b)), the errors of BEM become even more striking. The BEM Eq. (5) is supposed to give a linear plot of $1/\sigma_N^2$ versus D, but linear regression of the data (Fig. 10(b)) gives a very poor fit (solid line), with correlation coefficient $\rho^2=0.67$. By contrast, the SEL Type 1 gives (in the linear regression plot of σ_N^r versus $1/D$, $r=2$) an excellent fit, with ρ^2

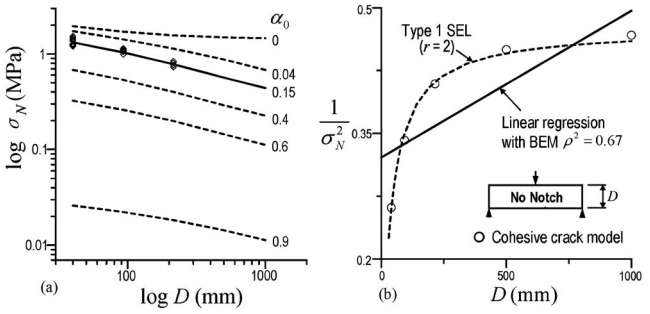

Fig. 10. (a) Nominal strength values obtained by cohesive crack model for various α_0 (data points: individual tests); (b) linear regression according to BEM for no notch ($\alpha_0=0$) of computer results by cohesive crack model

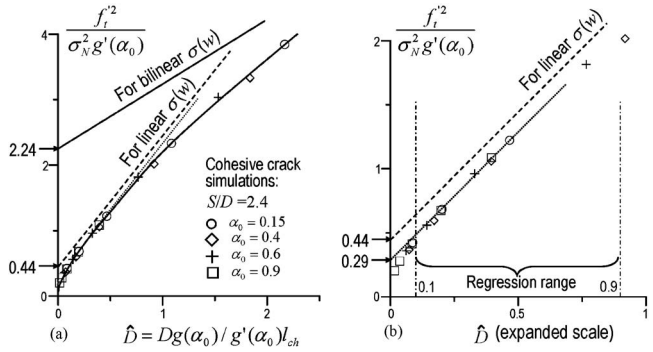

Fig. 11. Dimensionless plots of size effect simulations by cohesive crack model and their asymptotes

=0.99 (dashed curve in Fig. 10(b)). For comparison also note that, for $\alpha_0=0.15$, the SEL Type 2 regression gives $\rho^2=0.99$.

Aside from the data points of the new test results, Fig. 10 shows in logarithmic scale the simulated size effect curves for notches ranging from $\alpha_0=0$ to $\alpha_0=0.9$ and D up to 1 m. Note that the upper dashed curve for $\alpha=0$ closely approaches a horizontal asymptote, as required by the deterministic Type 1 SEL, whereas the BEM Eq. (5) would in the plot of Fig. 10 give a straight line of slope $-1/2$. The impossibility of this slope is also documented in Fig. 8(d), which compares the simulated stress profiles at peak loads for notchless beams of $D=40$ mm and 1,000 mm. For size $D=1{,}000$ mm the stress profile is almost linear, which implies that the deterministic size effect must disappear for larger sizes. Obviously, Eq. (5) of the BEM is unrealistic.

Identification of Tensile Strength from Size Effect Data

The material tensile strength (discussed in Item 11) can be determined from Irwin's relation as

$$f_t' = \sqrt{EG_f/l_{\text{ch}}}, \quad l_{\text{ch}} = c_f/\gamma \tag{9}$$

The problem is to find the ratio $\gamma=c_f/l_{\text{ch}}$ and to decide whether to use the initial fracture energy G_f or the total one, G_{fT}. This problem has been illuminated by cohesive crack simulations of Bažant et al. (2002) and especially Cusatis and Schauffert (2009). Type 2 linear regression delivers the value of l_{ch}, but the regression line is only approached for $D\to\infty$. For decreasing D, the cohesive crack results deviate from the regression line appreciably [Fig. 11(a)], and the proper correction must be figured out.

Another problem to address is that, for bilinear softening (Fig. 8), two different asymptotes can be defined: one for G_f, and one for G_{fT} [Fig. 11(a)]. Because of the long tail of $\sigma(w)$, the asymptote for G_{fT} (bilinear softening) is closely approached only for specimen sizes far beyond the laboratory range [and outside Fig. 11(a)], precisely for $\hat{D}>10$ where $\hat{D}=Dg(\alpha_0)/l_{\text{ch}}g'(\alpha_0)$ =dimensionless shape-independent size. When the tail is ignored and only the steep linear softening is considered, there is a steeper asymptote, which is approached closely for sizes an order of magnitude smaller. Cusatis and Schauffert (2009) find that the asymptotic slope corresponding to G_f is best obtained by tests within the range $\hat{D}\in(0.2,0.7)$.

However, this optimal size range is obtained by cohesive crack model only if the randomness of tests is not considered. To reduce the inevitable random scatter of regression slope in data fitting, it is statistically preferable that the size range be at least 1:8 (Bažant and Planas 1998). Therefore, the size range of at least $\hat{D}\in(0.1,0.9)$ is desirable.

To extend the testing range, the program for the cohesive crack model was run for notched specimens with $\alpha=0.04$, 0.15, 0.4, 0.6, 0.9, and sizes $D=40$, 93, 215, and 500 mm. The parameters of SEL (Type 2) and BEM [Eqs. (1) and (5)], obtained by linear regression of the σ_N values computed with the cohesive crack model, are listed in Table 1 and compared in Fig. 12. But no SEL parameters are listed for $\alpha\le0.04$ because SEL is not applicable in that range. For notchless beams, an imaginary notch $\alpha=0.02$, based on the ratio of maximum aggregate size to the largest D, is assumed for BEM calculations.

For SEL, f_t' is calculated in Table 1 from Eq. (9) using the value $\gamma=0.29$ [Fig. 11(b)]. Computer simulations show that 0.29 gives good results (much better than BEM) for all 3PB beams with typical span-to-depth ratios (2.4–8) and medium notch

Table 1. Material Parameters Obtained by Regression of Nominal Strength Values Obtained by Cohesive Crack Model

	Cohesive crack model				Size effect law				BEM		
α_0	K_{IC}	G_f	f_t'	G_{fT}	K_{IC}	G_f	f_t'	c_f	$A(\alpha)$	K_{IC}	f_t'
0	0.98	32	4.8	64	—	—	—	—	0.96	1.53	6.96
0.04	″	″	″	″	—	—	—	—	0.92	0.88	7.28
0.15	″	″	″	″	0.996	33.1	5.00	11.1	0.72	0.996	7.88
0.40	″	″	″	″	1.01	33.8	4.68	12.96	0.36	1.01	8.15
0.60	″	″	″	″	0.969	31.3	4.98	10.58	0.16	0.969	8.58
0.90	″	″	″	″	0.869	25.2	5.98	5.91	0.01	0.869	9.99

Note: An artificial $\alpha_0=0.02$ is selected for unnotched beams for the BEM.

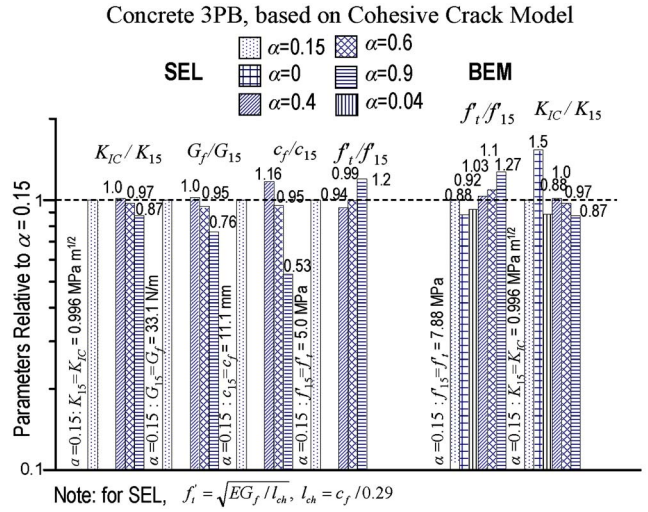

Fig. 12. Comparison of the results of SEL and BEM with cohesive crack model

depths ($0.15 \leq \alpha \leq 0.6$); see Table 1. In Fig. 11(b), γ gives the intercept of the regression line.

The wide applicability of intercept $\gamma = 0.29$ turns out to be a lucky coincidence due to the long tail of $\sigma(w)$. If the softening law $\sigma(w)$ were linear (no tail), the asymptote would give factor $\gamma = 0.44$ [Fig. 11(b)], as already found by Cusatis and Schauffert (2009). But this asymptote is approached closely only for unacceptably large D ($\hat{D} > 10$). By virtue of the transition to the second asymptote for G_{fT} of bilinear $\sigma(w)$ [Fig. 11(a)], it luckily happens that, in the normal testing range $0.2 \leq \hat{D} \leq 0.7$, the curve in Fig. 11 computed from the cohesive crack model is virtually parallel to the asymptote for initial linear softening giving the value of G_f. The downward shift from this asymptote [which actually represents the "intermediate asymptote" in the sense of Barenblatt (1996,2003)] amounts to a change of γ from 0.44 to 0.29 [Fig. 11(b)]. It is for this reason that the SEL regression of σ_N data from the cohesive crack model yields excellent agreement for G_f, as well as l_{ch} and f_t' (Table 1).

Nevertheless, if the size range of specimens is extended to $\hat{D} \in (0.1, 0.9)$, which helps to minimize the scatter of the regression slope of test data, the results of regression for G_f are almost same. But for c_f and f_t' it is then better to reduce γ to 0.28, in order to compensate for the small downward shift of the regression line due to the curvature of the plot outside the interval (0.2,0.7). A proper adjustment of γ according to Fig. 11 would permit even broader size ranges, such as 1:16.

As seen in Table 1, the scatter of f_t' values over the full range of α_0 is significant for the BEM, even though it claims to cover all notch depths. On the other hand, the SEL based testing of G_f, c_f, and f_t' gives acceptable results for $0.15 \leq \alpha_0 \leq 0.6$, which is in the recommended testing range. For $\alpha_0 = 0.04$ and 0.9, which are not within the recommended range of SEL testing, the regression results deviate from the cohesive crack model considerably. However, the estimates of G_f, c_f for specimen sizes $0.2 < \hat{D} < 0.7$ are good. The reason is that, in the dimensionless plot of $(f_t'/\sigma_N)^2/g'$ versus $\hat{D}$, they share the same curve with $0.15 \leq \alpha \leq 0.6$; see Fig. 11.

As for the BEM, the picture is different. First, the BEM testing of K_{IC} and f_t' is supposed to be made at various α_0 for one size only. So, not surprisingly, the scatter seen in Table 1 is much larger than it is for the SEL. This is a serious deficiency of the BEM testing method. Contrary to the opinion of Hu and Duan, testing at different sizes cannot be avoided, as already concluded in Tang et al. (1996), and the reason is that a sufficient range of brittleness numbers $\beta = D/D_0$ can never be attained by merely varying the notch depth at constant size (Tang et al. 1996). The f_t' values obtained by BEM severely disagree with the cohesive crack model for every notch depth (Table 1). For the extremes $\alpha = 0$ and 0.9, they are 6.96 MPa and 10.0 MPa, respectively, although the central hypothesis of the BEM is that extremely shallow and extremely deep notches should have the same asymptote, with $\sigma_n \to f_t'$. The BEM generally overestimates f_t' by about 70%. This observation also strengthens the objection that the small-size asymptote of the BEM based on linear stress profile across the ligament is fundamentally unjustifiable. Thus it must be concluded that the BEM testing method cannot give a realistic tensile strength.

Note in Table 1 that parameter G_f obtained from linear regression of Eq. (1) differs only marginally from the initial fracture energy G_f of the cohesive crack model; e.g., $G_f = 33.8$ N/m for $\alpha_0 = 0.4$, which is about 5% larger. This difference is less than the inevitable randomness of tests. For the tensile strength f_t', too, the difference is $<5\%$. This small discrepancy, which was discussed before (Bažant et al. 2002; Cusatis and Cedolin 2007; Cedolin and Cusatis 2008), is explained by the fact that the present tests, as well as many previous tests, were carried out for a size range slightly shifted to the left of the optimal size range $0.2 < \hat{D} < 0.7$ (Cusatis and Schauffert 2009), for which the exact asymptotic slope is obtained. Consequently, in view of the curvature of the data point series in Fig. 11(b), the slope of the regression line of the σ_N values was slightly higher or lower than the asymptotic slope, thus giving a slightly lower or higher G_f.

For $\alpha_0 = 0.04$, aside from the deviation introduced by using small sizes, there is another source of error. As illustrated in Fig. 10, there exists a transition from unnotched tests to notched tests. Therefore, the nominal strength will approach the Type 1 size effect for small size beams with a shallow notch. When $D = 40$ and 93 mm, the crack length is 1.6 and 3.7 mm, respectively, which is far less than the maximum aggregate size (9.5 mm) and should not be treated as an effective notch. If the nominal strengths for these shallow notches are removed from the regression, G_f and f_t' will be significantly improved, from 26.0 N/m and 5.35 MPa to 29.0 N/m and 4.70 MPa, respectively.

When the size is large enough ($\hat{D} > 0.1$, though not $\hat{D} > 0.9$), the BEM will generate a consistent f_t' for notched beams. However the $f_t' = 8.2$ MPa is very different from the cohesive tensile strength $f_t' = 4.80$ MPa. If the beam is sufficiently small, the cohesive crack model shows that a plastic glue with yield strength f_t' can be assumed to replace the cohesive zone along the crack line (Bažant et al. 2002). Hence, for a 3PB beam, one can obtain $B = 2D(1-\alpha_0)^2/S$, where S is the span. Using cohesive crack model to simulate an extremely small specimen to obtain the σ_N, i.e., $\sigma_N = 2.7$ MPa for $D = 0.1$ mm and $\alpha_0 = 0.15$, one can calculate $f_t' = 4.5$ MPa, close to the cohesive tensile strength. With the help of the cohesive crack model, the parameters obtained from Eq. (1) are more solidly justified.

Main Conclusions

1. The basic BEM hypothesis that the size effect is caused by interaction of the FPZ with the boundary is unjustified.

2. The BEM provides realistic values of K_{IC} and G_f, almost as good as the SEL values, provided that only the basic Mode I fracture specimen geometries are used, the range is restricted to $\alpha_0 \in (0.15, 0.60)$, and the sizes are within the range $\hat{D} \in (0.1, 0.9)$. Outside these ranges, the BEM results for K_{IC} and G_F have unacceptable errors. Unlike the SEL, the BEM is invalid for mixed mode, shear and torsional fracture specimens, and generally for engineering structures.
3. The linear stress profile assumed in the BEM is a source of large error outside the aforementioned ranges, and precludes applications to general structures, or to other than the simplest test specimens (Fig. 1).
4. The BEM representation of size effect in notchless specimens is unrealistic, and so is the hypothesis of the largest material flaw being proportional to the specimen size.
5. Another deficiency is that the BEM does not converge to the Weibull statistical theory for large notchless specimens.
6. The BEM cannot provide correct values of material tensile strength f_t'. The error is about 70%.
7. The fracture energy G_F obtained with the BEM is not the total fracture energy G_{fT} but the initial fracture energy G_f.
8. The SEL is extended to provide also the values of material tensile strength f_t'.
9. Testing the size effect on peak loads for two significantly different relative notch depths, such as $\alpha_0 = 0.15$ and 0.60, improves the SEL test results and allows limiting the size range to about 1:4. This reinforces the previous conclusion of Tang et al. (1996).
10. Measurement of f_t' and calibration of the cohesive crack model with bilinear $\sigma(w)$ requires that the size effect tests be supplemented by measurement of nearly complete load-CMOD curves for at least the largest specimens. Then the SEL testing yields not only the initial but also the total fracture energy.

Acknowledgments

Support by the U.S. DoT through a Grant No. 20778 from the Infrastructure Technology Institute of Northwestern University is gratefully acknowledged.

References

Barenblatt, G. I. (1959). "The formation of equilibrium cracks during brittle fracture, general ideas and hypotheses, axially symmetric cracks." *Prikl. Mat. Mech.*, 23(3), 434–444.

Barenblatt, G. I. (1996). *Scaling, selfsimilarity, and intermediate asymptotics*, Cambridge University Press, Cambridge, U.K.

Barenblatt, G. I. (2003). *Scaling*, Cambridge University Press, Cambridge, U.K.

Bažant, Z. P. (1984). "Size effect in blunt fracture: Concrete, rock, metal." *J. Eng. Mech.*, 110(4), 518–535.

Bažant, Z. P. (1996). "Analysis of work-of-fracture method for measuring fracture energy of concrete." *J. Eng. Mech.*, 122(2), 138–144.

Bažant, Z. P. (1997). "Scaling of quasibrittle fracture: Asymptotic analysis." *Int. J. Fract.*, 83(1), 19–40.

Bažant, Z. P. (2001). "Size effects in quasibrittle fracture: Apercu of recent results." *Proc., FraMCoS-4 Int. Conf.*, R. de Borst, J. Mazars, G. Pijaudier-Cabot, and J. G. M. van Mier, eds., Balkema, Rotterdam, The Netherlands, 651–658.

Bažant, Z. P. (2004). "Scaling theory of quaisbrittle structural failure." *Proc. Natl. Acad. Sci. U.S.A.*, 101(37), 13400–13407.

Bažant, Z. P. (2005). *Scaling of structural strength*, 2nd Ed., Elsevier, London.

Bažant, Z. P., and Becq-Giraudon, E. (2002). "Statistical prediction of fracture parameters of concrete and implication for choice of testing standard." *Cem. Concr. Res.*, 32(4), 529–556.

Bažant, Z. P., and Kazemi, M. T. (1990a). "Determination of fracture energy, process zone length, and brittleness number from size effect, with application to rock and concrete." *Int. J. Fract.*, 44, 111–131.

Bažant, Z. P., and Kazemi, M. T. (1990b). "Size effect in fracture of ceramics and its use to determine fracture energy and effective process zone length." *J. Am. Ceram. Soc.*, 73(7), 1841–1853.

Bažant, Z. P., Le, J.-L., and Bazant, M. Z. (2009). "Scaling of strength and lifetime probability distributions of quasibrittle structures based on atomistic fracture mechanics." *Proc. Natl. Acad. Sci. U.S.A.*, 106(28), 11484–11489.

Bažant, Z. P., and Li, Z. (1996). "Zero-brittleness size-effect method for one-size fracture test of concrete." *J. Eng. Mech.*, 122(5), 458–468.

Bažant, Z. P., and Novák, D. (2000a). "Probabilistic nonlocal theory for quasibrittle fracture initiation and size effect. I. Theory." *J. Eng. Mech.*, 126(2), 166–174.

Bažant, Z. P., and Novák, D. (2000b). "Probabilistic nonlocal theory for quasibrittle fracture initiation and size effect. II. Application." *J. Eng. Mech.*, 126(2), 175–185.

Bažant, Z. P., and Pang, S.-D. (2006). "Mechanics based statistics of failure risk of quasibrittle structures and size effect on safety factors." *Proc. Natl. Acad. Sci. U.S.A.*, 103(25), 9434–9439.

Bažant, Z. P., and Pang, S.-D. (2007). "Activation energy based extreme value statistics and size effect in brittle and quasibrittle fracture.'" *J. Mech. Phys. Solids*, 55, 91–134.

Bažant, Z. P., and Pfeiffer, P. A. (1987). "Determination of fracture energy from size effect and brittleness number." *ACI Mater. J.*, 84, 463–480.

Bažant, Z. P., and Planas, J. (1998). *Fracture and size effect in concrete and other quasibrittle materials*, CRC, Boca Raton, Fla.

Bažant, Z. P., Vořechovský, M., and Novák, D. (2007). "Asymptotic prediction of energetic-statistical size effect from deterministic finite element solutions." *J. Eng. Mech.*, 133, 153–162.

Bažant, Z. P., and Xi, Y. (1991). "Statistical size effect in quasi-brittle structures: II. Nonlocal theory." *J. Eng. Mech.*, 117(7), 2623–2640.

Bažant, Z. P., and Yu, Q. (2004). "Size effect in concrete specimens and structures: New problems and progress." *Proc., FraMCoS-5, 5th Int. Conf. on Fracture Mech. of Concrete and Concr. Structures*, Vol. 1, V. C. Li, K. Y. Leung, K. J. Willam, and S. L. Billington, eds., IA-FraMCos, Evanston, Ill., 153–162.

Bažant, Z. P., and Yu, Q. (2009). "Universal size effect law and effect of crack depth on quasi-brittle structure strength." *J. Eng. Mech.*, 135(2), 78–84.

Bažant, Z. P., Yu, Q., and Zi, G. (2002). "Choice of standard fracture test for concrete and its statistical evaluation." *Int. J. Fract.*, 118, 303–337.

Cedolin, L., and Cusatis, G., (2008). "Identification of concrete fracture parameters through size-effect experiments." *Cem. Concr. Res.*, 30, 788–797.

Cusatis, G., and Cedolin, L. (2007). "Two-scale analysis of concrete fracturing behavior." *Eng. Fract. Mech.*, 74, 3–17.

Cusatis, G., and Schauffert, E. A. (2009). "Cohesive crack analysis of size effect." *Eng. Fract. Mech.*, 76, 2163-2173.

Duan, K., and Hu, X. (2004). "Specimen boundary induced size effect on quasi-brittle fracture." *Strength, Fracture, and Complexity*, 2(2), 47–68.

Duan, K., Hu, X., and Wittmann, F. (2006). "Scaling of quasi-brittle fracture: Boundary and size effect." *Mech. Mater.*, 38, 128–141.

Freudenthal, A. M. (1968). "Statistical approach to brittle fracture." *Fracture: An advanced treatises*, Vol. 2, H. Liebowitz, ed., Academic, New York, 591–619.

Hillerborg, A. (1985). "The theoretical basis of a method to determine the fracture energy G_F of concrete." *Mater. Struct.*, 18, 291–296.

Hillerborg, A., Modéer, M., and Petersson, P. E. (1976). "Analysis of

crack formation and crack growth in concrete by means of fracture mechanics and finite elements." *Cem. Concr. Res.*, 6, 773–782.

Hu, X. (2002). "An asymptotic approach to size effect on fracture toughness and fracture energy of composites." *Eng. Fract. Mech.*, 69, 555–564.

Hu, X., and Duan, K. (2007). "Size effect: Influence of proximity of fracture process zone to specimen boundary." *Eng. Fract. Mech.*, 74, 1093–1100.

Hu, X., and Duan, K. (2008). "Size effect and quasi-brittle fracture: The role of FPZ." *Int. J. Fract.*, 154, 3–14.

Hu, X., and Duan, K. (2010). "Mechanism behind the size effect phenomenon." *J. Eng. Mech.*, 136(1), 60–68.

Hu, X., and Wittmann, F. (2000). "Size effect on toughness induced by crack close to free surface." *Eng. Fract. Mech.*, 65, 209–221.

Irwin, G. R. (1958). "Fracture." *Handbuch der physik*, Vol. 6, S. Flügge, ed., Springer, Berlin, 551–590.

Karihaloo, B. L., Abdalla, H. M., and Xiao, Q. Z. (2003). "Size effect in concrete beams." *Eng. Fract. Mech.*, 70, 979–993.

Nakayama, J. (1965). "Direct measurement of fracture energies of brittle heterogeneou material." *J. Am. Ceram. Soc.*, 48(11), 583–587.

Petersson, P. E. (1981). "Crack growth and development of fracture zone in plain concrete and similar materials." *Rep. No. TVBM-1006*, Div. of Building Materials, Lund Institute of Technology, Lund, Sweden.

Rice, J. R. (1968). *Mathematical analysis in the mechanics of fracture—An advanced treatise*, Vol. 2, H. Liebowitz, ed., Academic, New York, 191–308.

RILEM. (1985). "Determination of the fracture energy of mortar and concrete by means of three-point bend tests on notched beams." *Mater. Struct.*, 18, 285–290.

RILEM TC QFS. (2004). "Quasibrittle fracture scaling and size effect—Final report." *Mater. Struct.*, 37(272), 547–586.

Tang, T., Bažant, Z. P., Yang, S., and Zollinger, D. (1996). "Variable-notch one-size test method for fracture energy and process zone length." *Eng. Fract. Mech.*, 55(3), 383–404.

Tattersall, H. G., and Tappin, G. (1966). "The work of fracture and its measurement in metals, ceramics and other materials." *J. of Materials Society*, 1(3), 296–301.

Weibull, W. (1939). "The phenomenon of rupture in solids." *Proc., Royal Swedish Institute of Engineering Research*, Vol. 153, Ingenioersvetenskaps Akad. Handl., Stockholm, 1–55.

Weibull, W. (1951). "A statistical distribution function of wide applicability." *ASME J. Appl. Mech.*, 18, 293–297.